Article

Kinetic Studies on Gas-Based Reduction of Vanadium Titano-Magnetite Pellet

Junwei Chen [1], Liang Mi [1], Yang Jiao [1] and Xidong Wang [1,*]

[1] Department of Energy and Resources Engineering, College of Engineering, Peking University, Beijing 100871, PR China; 1401111582@pku.edu.cn (J.C.); liangmicoming@163.com (M.L.); jiaoyang518@foxmail.com (Y.J.); xidong@pku.edu.cn (X.W.)

* Correspondence: xidong@pku.edu.cn (X.W.)

Abstract: Vanadium titano-magnetite is a significant resource in China, and in this study, we characterize its isothermal reduction mechanisms in the mixture of H_2, CO, and N_2 where the variables considered here include reduction time, reduction temperature, gas composition, and pellet size. The kinetics of the reduction process are mainly studied, which follows a shrinking core model. The results indicate that the reduction degree of oxidized VTM pellets increases with the increase of reduction time, reduction temperature but decreases with the increase of pellet size. Moreover, we found that an increase of $H_2/(H_2+CO)$ ratio induces an increase of the reduction degree. Then the transformation of main Ti-bearing mineral phases is discussed, and the most probable reaction mechanism is revealed. In the whole reduction process, the kinetic results confirm the existence of an early stage and a latter stage, which are controlled by interface chemical reaction and diffusion, respectively. Furthermore, the results show that the diffusion-control step can be observably shortened with the decrease of pellet size because a thinner product layer is formed during the reduction process. Our study thus provides a valuable technical basis on the VTM industrial application.

Keywords: Vanadium titano-magnetite; gas-based reduction; carbon monoxide; hydrogen; kinetics; pellet size

1. Introduction

Vanadium titano-magnetite (VTM) is a kind of multi-elements-coexistent mineral, which contains iron (Fe), titanium (Ti), vanadium (V) and varieties of rare metals [1,2]. VTM is becoming increasingly important because of its significant value in the high-tech industries [3]. According to statistics, more than ten billion tons VTM resource are stored in China. The abundant reserves ranks China in the third in the world, following behind Russia and South Africa [4,5]. The VTM with TiO_2 and V_2O_5 is abundant in Panxi Area of China, where the amount of TiO_2 and V_2O_5 account for more than 90% and 80% of the total quantity all over China, respectively [6-8]. Hence, it is important to utilize the VTM in Panxi Area of China for the better supplement of Ti and V.

The crystalline structure of VTM is complicated because the Ti and Fe are symbiosis closely to each other in the ore, and V is as isomorphism hosting in the lattice of VTM [9]. The key to utilize those resource is that how to separate the Fe, V and Ti efficiently. The processes of utilizing VTM fall into two categories: blast furnace (BF) process or non-BF processes [10,11]. The BF technology is widely recognized because it has been developed for a long time in China and Russia. But some problems can exist at same time. Firstly, the continuous shortage of coke resource limits development of BF technology. Besides, the introduction of limestone as a kind of solvent in blast furnace decreases the grade of TiO_2, and the reaction of TiO_2 with limestone to produce perovskite leads to almost no recycling of titanium in VTM. Currently, many researches have been conducted on the comprehensive utilization of VTM by non-BF processes, and a few technological processes for the

Preprints (www.preprints.org) | NOT PEER-REVIEWED | Posted: 30 October 2018 doi:10.20944/preprints201810.0723.v1

utilization of VTM have already been developed. The pre-reduction electric furnace smelting process is the most promising processes because of the high recovery rates of valuable elements and low costs [9].

Reduction is an essential procedure in the pre-reduction electric furnace smelting process. Hence, it is extremely important to investigate the reduction behavior and kinetics of VTM. In recent decades, a large number of researches have been carried out to investigate reduction behavior and kinetics of VTM. Most previous research of reduction behavior and kinetics of VTM was mainly focused on the process that using coal as the reducing agent [6,7,12-16]. However, the rate of the reduction reaction is relatively slow in coal-based reduction process. In addition, with political pressure on environmental protection, gas-based reduction of VTM is playing a more and more important role. Compared with coal-based reduction, gas-based reduction has a large number of obvious advantages such as higher reduction degree, better processing capacity as well as less pollution [9,10,17-20]. Although a few papers deal with the gas-based reduction of VTM, there are two important problems in the previous research on the gas-based reduction behavior and kinetics of VTM. Firstly, many reduction experiments were based on pure hydrogen (H_2) or pure carbon monoxide (CO). Nevertheless, most of the reactions is between the VTM and the gas mixture of CO, H_2 and N_2 in the actual industrial process. Secondly, the previous study did not consider the particle size of oxidized VTM pellets, which can play an important role in the reduction kinetics. Therefore, previous experiments were not carried out by simulating the actual reduction gas, which are difficult to guide the VTM industrial application.

In this paper, the gas-based reduction kinetics of oxidized VTM pellets was studied systematically. The effects of reduction time, reduction temperature, gas composition of different $H_2/(H_2+CO)$ ratios with 25% N_2, and pellets size on the VTM reduction kinetics were studied by using unreacted nuclear shrinkage model. Our study is expected to provide a more valuable technical basis on the VTM industrial application.

2. Materials and Methods

2.1. Preparation of oxidized VTM pellets

The VTM sample used in this study was obtained from the Paixi Area of China. The XRD patterns of the VTM are shown in **Figure 1(a)**. As can be seen from **Figure 1(a)**, the main mineral phases of the VTM are magnetite (Fe_3O_4) and Ilmenite ($FeTiO_3$). Elements Ti and Fe are symbiosis closely to each other in the mineral phase.

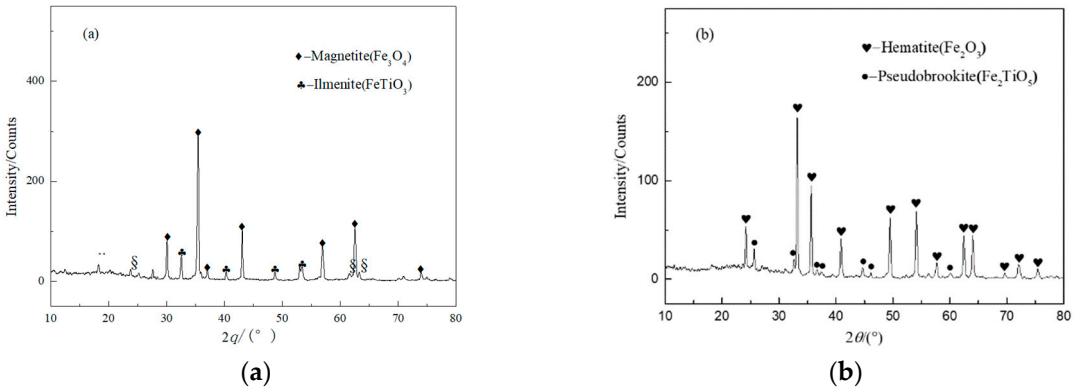

(**a**) (**b**)

Figure 1. XRD patterns of the sample: (a) the VTM; (b) the oxidized VTM pellets.

The oxidized VTM pellets were prepared as follows. The VTM was fully mixed with 1 wt% binder and 8.5 wt% water and then pelletized to the diameter of 6-8 mm, 8-10 mm, 10-12 mm, 12-14 mm, and 14-16 mm in a disc pelletizer, respectively. Then, the VTM pellets were loaded into a quartz reactor after being dried at the temperature of 110°C for 4 h. Finally, the VTM pellets were calcined at the temperature of 1350°C for 20 min under the air condition. The main chemical compositions are

Preprints (www.preprints.org) | NOT PEER-REVIEWED | Posted: 30 October 2018 doi:10.20944/preprints201810.0723.v1

displayed in **Table 1**, while the XRD patterns of the oxidized VTM pellets are shown in **Figure 1 (b)**. It can be seen that the main mineral phases of oxidized VTM pellets were hematite (Fe_2O_3) and pseudobrookite (Fe_2TiO_5). It can be concluded that Fe_3O_4 and $FeTiO_3$ transformed to hematite Fe_2O_3 and Fe_2TiO_5 during the pre-oxidation process.

Table 1. Main chemical compositions of oxidized VTM pellets (wt%).

TFe	FeO	TiO_2	SiO_2	Al_2O_3	MgO	CaO	V_2O_5	MnO	S
45.50	0.59	13.40	8.42	6.54	3.28	1.40	0.54	0.32	0.037

2.2. Experimental measurements

In this study, 200 g heated oxidized VTM pellets directly react with reducing gas in the furnace. The experimental equipment in this work was shown in **Figure 2**, mainly composed of reducing gas flow control cabinet, tube furnace, high temperature resistant reactor made of steel alloy, coal gas analyzer, electronic balance and computer.

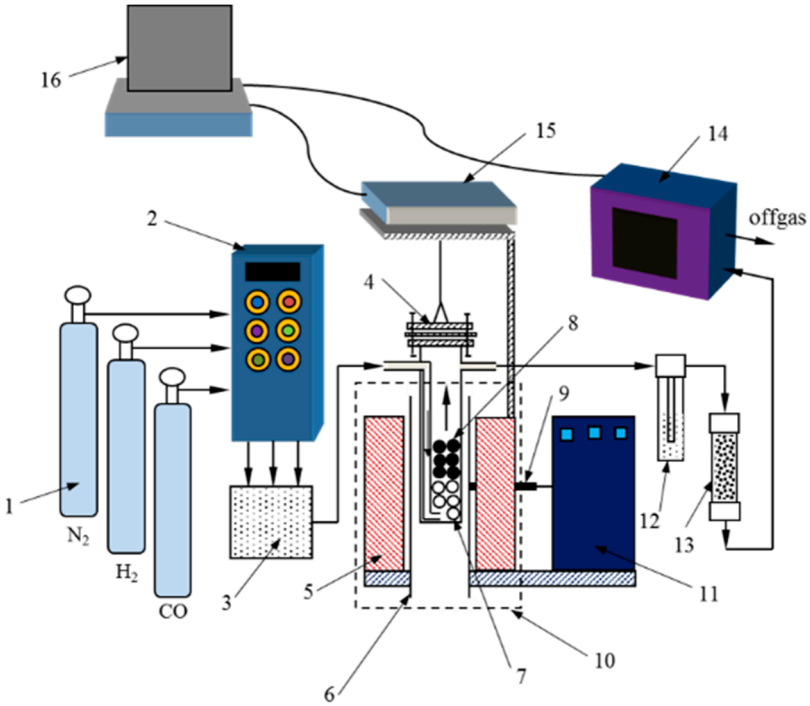

Figure 2. Schematic of the experimental apparatus: 1-gas cylinder, 2-flow control cabinet, 3-gas mixing chamber, 4-reactor, 5-fever zone, 6-alundum tube, 7-corundum ball, 8-oxidized VTM pellets, 9- thermocouple, 10-tube furnace, 11-temperature controlling cabinet, 12-wash bottle, 13-drying bottle, 14-coal gas analyzer, 15-electronic balance, 16-computer.

Firstly, 400 g corundum balls with average diameter of 1 cm were placed at the bottom of the reactor to disperse the reducing gases, and the oxidized VTM pellets were laid above the corundum balls evenly. A gasket made of silica gel was placed between the flanges to improve the air tightness of the reactor at the same time. Then the blind flange of the reactor was closed. The inlet pipe and the exit pipe were connected with the reactor and the reactor was filled with N_2 to check the air tightness. With well air tightness, the reactor was suspended on the bottom of the electronic balance placed above the tube furnace. Later, the power of the tube furnace was turned on, the temperature program was settled down and the heater was turned up. In the whole heating process, the N_2 was full of the reactor. When the temperature rose to a specified temperature, the electronic balance and the coal gas analyzer were turned on and began to record the data. Then, the N_2 was replaced by the reducing gas

Preprints (www.preprints.org) | NOT PEER-REVIEWED | Posted: 30 October 2018 doi:10.20944/preprints201810.0723.v1

to carry out the reduction. After that, the N_2 was switched back. Finally, the sample was taken out from furnace the after cooled down.

H_2, CO and N_2 controlled by flow-controlled cabinet were fully mixed in the mixing chamber in the reduction reaction，and the reaction pressure was 1 atm. Then the gas mixture got into the bottom of the reactor straightly through the inlet pipe along the inwall of reactor. After that, the reducing gas mixture met with the oxidized VTM pellets. The data of mass change was recorded by the electronic balance continuously, was transferred to the computer and was stored in the computer. It is critical to remove the dust and vapor in the offgas completely for avoiding the damage of the coal-gas analyzer. Thus, the offgas firstly entered into the water-wash bottle and then got through the drying bottle. Later, we measured the chemical components of offgas online continuously by the coal-gas analyzer and stored the data in the computer. Finally, the off-gas was emptied. After the samples being reduced for 240 min, the VTM pellets were cooled to room temperature under a N_2 atmosphere for later testing.

The reduction degree of oxidized VTM pellets can be calculated as follows [9]:

$$R = \frac{m(O_L)}{m_0(O_L)} = \left(\frac{0.11w(FeO)}{0.43w(TFe)} + \frac{m_1 - m_2}{m_1 \times 0.43w(TFe)}\right) \times 100\% \quad (1)$$

in which R is reduction degree of iron, $m_0(O_L)$ is the total weight of O which bond with Fe in oxidized VTM pellets, $m(O_L)$ is the weight loss of O which bond with Fe during reduction, $w(TFe)$ and $w(FeO)$ are the mass fraction of TFe and FeO in oxidized VTM pellets, m_1 is the mass of the VTM pellet before reduction, m_2 is the mass of the VTM pellet in reduction process. 0.11 and 0.43 represent the oxygen demand conversion coefficient when converting FeO and Fe to Fe_2O_3, respectively.

2.3. Reduction kinetics analysis

Based on the earlier researches [9,10], it can be concluded that the reduction of the oxidized VTM pellets proceed topochemically. Therefore, the used kinetic model to describe the iron ore reduction is the un-reacted shrinking core model in this study, which includes the process of external diffusion of gaseous species, intrinsic chemical reaction and the diffusion of gas species. Under the condition of the mixture of H_2, CO and N_2 atmosphere, the total reduction time can be calculated according to the Eq. (2), which is based on the un-reacted shrinking core model. Therefore, the rate equations can be obtained as shown in Eq. (3) and Eq. (4). According to Eq. (3) and Eq. (4), multiple graphs can be drawn to investigate the actual rate-controlling step of the reduction process. If the process is the intrinsic chemical reaction controlled, the plot of $1-(1-R)^{\frac{1}{3}}$ vs. time should be a straight line. For the diffusion of gas species controlling step, the plot of $1-\frac{2}{3}R-(1-R)^{\frac{2}{3}}$ vs. time should be a straight line. In the Eq. (2), Eq. (3) and Eq. (4), t is the total reduction time (min), k is the reduction rate constant (cm/min), r_0 is characteristic initial radius of the pellet (cm), ρ_0 is initial oxygen concentration in the pellet (mol/cm^3), k_0 is the parameter constant, c_0 and c_q are reduction gas concentration at granule surface and in equilibrium respectively (mol/cm^3), D_e is the effective diffusion coefficient (cm^2/min).

$$t = \frac{r_0\rho_0}{k_0(c_0-c_q)}\left[1-(1-R)^{\frac{1}{3}}\right] + \frac{r_0^2\rho_0}{D_e(c_0-c_q)}\left[1-\frac{2}{3}R-(1-R)^{\frac{2}{3}}\right] \quad (2)$$

$$kt = 1-(1-R)^{\frac{1}{3}} \quad (3)$$

$$kt = 1-\frac{2}{3}R-(1-R)^{\frac{2}{3}} \quad (4)$$

3. Results and discussion

3.1. Reduction temperature

The reduction of VTM pellets was carried out in the temperature range of 973-1373 K with the intervals of 100 K. Other specific experimental conditions were controlled: the total gas flow was 5 L·min^{-1}, the proportion of N_2 was 25%, the proportion of H_2 and CO was 75% (the H_2/(H_2+CO)=1/2),

 doi:10.20944/preprints201810.0723.v1

the diameter of oxidized VTM pellets was 10-12 mm. The experimental results are shown in **Figure 3**.

It can be seen that the reduction degree of oxidized VTM pellets is gradually increased with the reduction time. Besides, the reduction degrees are 49.8%, 56.0%, 71.0%, 85.0% and 93.3% at 973 K, 1073K, 1173K, 1273 K and 1373 K for 80min in $H_2/(H_2+CO)=1/2$ atmosphere, respectively, indicating that the reaction temperature can also strongly influence the reduction rate of oxidized VTM pellets. The reduction degree can be greatly elevated with the increase of temperature because minerals crystal lattice has a high energy in high temperature. Besides, the H_2 and CO have higher reduction thermodynamic potential energy as the temperature increases. Thus, the reduction temperature of oxidized VTM pellets is recommended to exceed 1273 K in actual industrial production.

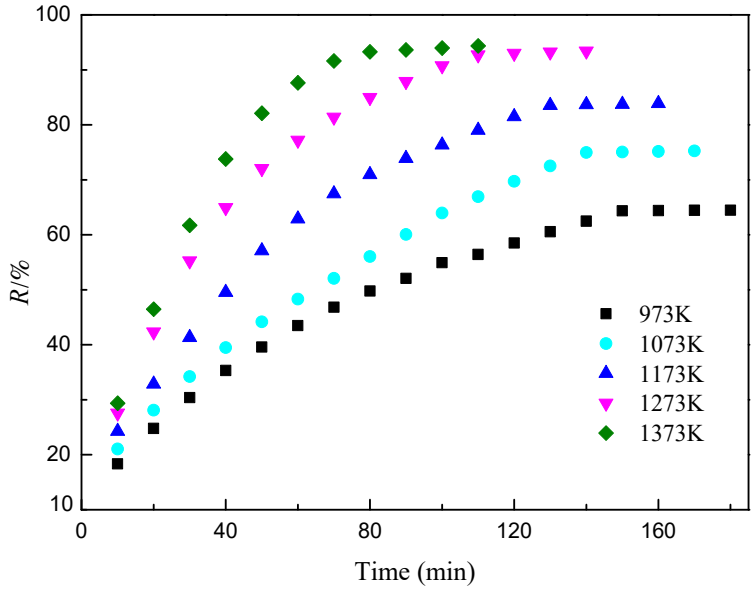

Figure 3. The reduction degree curves of oxidized VTM pellets at 973-1373 K in $H_2/(H_2+CO)=1/2$ atmosphere.

Preprints (www.preprints.org) | NOT PEER-REVIEWED | Posted: 30 October 2018 doi:10.20944/preprints201810.0723.v1

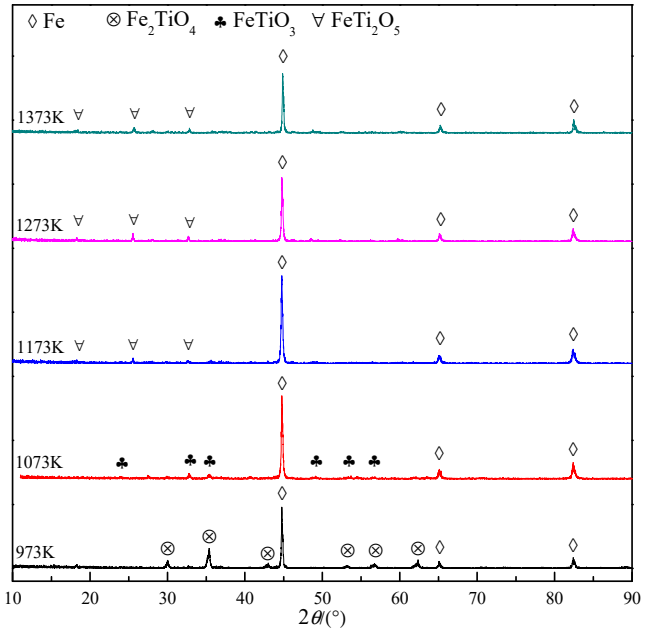

Figure 4. XRD patterns of the reduction products at 973 K-1373 K in $H_2/(H_2+CO)=1/2$ atmosphere.

Figure 4 shows the XRD patterns of the VTM pellets after the reduction process. The results reveal that Fe can be produced at 973 k-1373K. In addition, the Ti-bearing main mineral phase changes with the increase of temperature. The phase of Fe_2TiO_5 disappears and the phase of the reduction product is Fe_2TiO_4 at 973K. As the increase of temperature, Fe_2TiO_4 is reduced to $FeTiO_3$. With the temperature further increasing to 1173K, $FeTiO_3$ is reduced to $FeTi_2O_5$. Therefore, the most probable reaction mechanism of the reduction process can be described in Eq. (5-16).

$$3Fe_2O_3 + H_2(g) = 2Fe_3O_4 + H_2O(g) \quad (5)$$

$$Fe_3O_4 + H_2(g) = 3FeO + H_2O(g) \quad (6)$$

$$FeO + H_2(g) = Fe + H_2O(g) \quad (7)$$

$$3Fe_2O_3 + CO(g) = 2Fe_3O_4 + CO_2(g) \quad (8)$$

$$Fe_3O_4 + CO(g) = 3FeO + CO_2(g) \quad (9)$$

$$FeO + CO(g) = Fe + CO_2(g) \quad (10)$$

$$Fe_2TiO_5 + H_2(g) = Fe_2TiO_4 + H_2O(g) \quad (11)$$

$$Fe_2TiO_5 + CO(g) = Fe_2TiO_4 + CO_2(g) \quad (12)$$

$$Fe_2TiO_4 + H_2(g) = Fe + FeTiO_3 + H_2O(g) \quad (13)$$

$$Fe_2TiO_4 + CO(g) = Fe + FeTiO_3 + CO_2(g) \quad (14)$$

$$2FeTiO_3 + H_2(g) = Fe + FeTi_2O_5 + H_2O(g) \quad (15)$$

$$2FeTiO_3 + CO(g) = Fe + FeTi_2O_5 + CO_2(g) \quad (16)$$

On the basis of Eq. (3) and Eq. (4), kinetic results of the VTM pellets are shown in **Figure 5(a)** and **(b)**. It shows clearly that there are two stages in the whole reduction process: the early stage and the latter stage. The correlation coefficient (R^2) of the straight lines are 0.982, 0.998, 0.983, 0.985 and 0.986 at the early stage, respectively. The correlation coefficient (R^2) of the straight lines are 0.999, 0.998, 0.985, 0.993 and 0.997 at the latter stage, respectively. Thus, the great linear relationships

Preprints (www.preprints.org) | NOT PEER-REVIEWED | Posted: 30 October 2018 doi:10.20944/preprints201810.0723.v1

indicate that the reduction processes of the early stage and the latter stage are controlled by interface chemical reaction and diffusion, respectively. The values of the reduction rate constant of two stages are presented in **Table 2**. It is can be seen that the reduction rate constants of both the early stage and the latter stage increase with the elevated temperature. This indicates that the increase of temperature can effectively improve the reduction process.

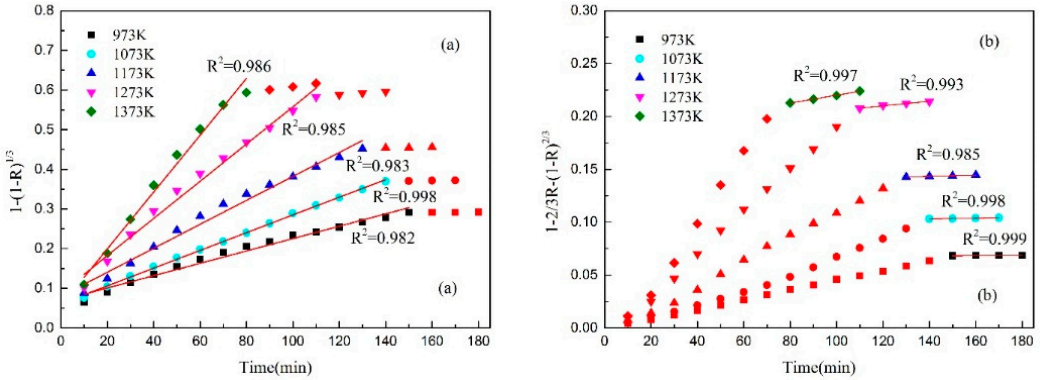

Figure 5. Plot of $1-(1-R)^{\frac{1}{3}}$ vs. time (a) and plot of $1-\frac{2}{3}R-(1-R)^{\frac{2}{3}}$ vs. time (b) at 973 K-1373 K in $H_2/(H_2+CO)$=1/2 atmosphere.

Table 2. The values of the reduction rate constant at 973 K-1373 K in $H_2/(H_2+CO)$=1/2 atmosphere.

temperature	973K	1073K	1173K	1273K	1373K
intrinsic chemical reaction control	0.00156	0.00224	0.00302	0.00469	0.00717
diffusion control	1.34E-05	3.88E-05	6.15E-05	2.13E-04	3.70E-04

According to the Arrhenius equation, the relationship between the reaction temperature (T) and the reduction rate constant (k) can be obtained as shown in Eq. (17). In Eq. (17), E is the activation energy (kJ·mol^{-1}), k_0 is the frequency factor.

$$k = k_0 \exp\left(-\frac{E}{RT}\right) \quad (17)$$

Taking the natural logarithm of both sides in Eq. (17):

$$\ln k = -\frac{E}{RT} + \ln k_0 \quad (18)$$

The plot of lnk vs. 1/T in $H_2/(H_2+CO)$=1/2 atmosphere is shown in **Figure 6 (a)** and **(b)**. The activation energies of intrinsic chemical reaction control stage and diffusion control stage can be evaluated based on the data of **Figure 6** and Eq. (18), and the calculated values are 41.65 KJ/mol and 92.45 KJ/mol, respectively. Therefore, the value of activation energy in intrinsic chemical reaction control stage is lower than that in diffusion control stage for gas-based reduction of oxidized VTM pellets.

Preprints (www.preprints.org) | NOT PEER-REVIEWED | Posted: 30 October 2018 doi:10.20944/preprints201810.0723.v1

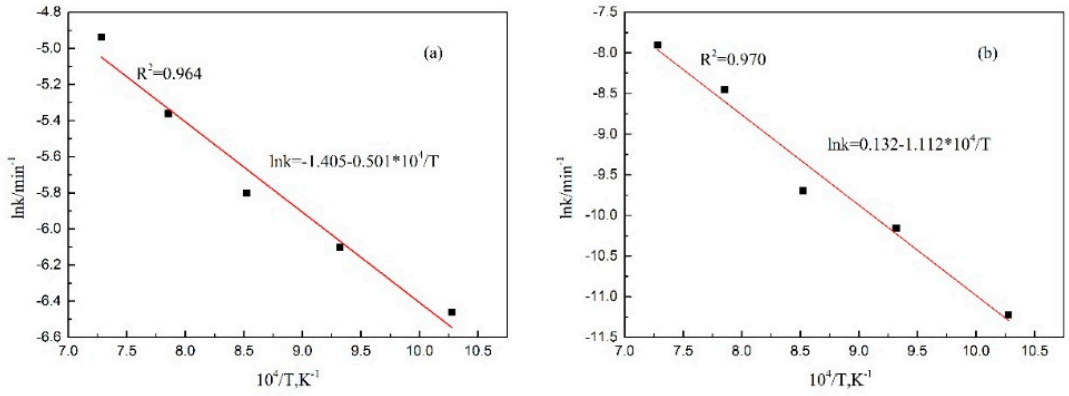

Figure 6. The Arrhenius plot of reaction degree constant k vs. temperature (a) intrinsic chemical reaction control step and (b) diffusion control step at 973 K-1373 K in $H_2/(H_2+CO)$=1/2 atmosphere.

3.2. Gas composition

To investigate the effect of gas composition on the reduction of oxidized VTM pellets, the experiment was carried out under the $H_2/(H_2+CO)$ ratios of 0, 1/4, 1/3, 1/2, 2/3, 3/4, and 1. Other specific experimental conditions were controlled: the reduction temperature was 1273K, the total gas flow was 3L·min^{-1}, the proportion of N_2 was 25%, the proportion of H_2 and CO was 75%, the oxidized VTM pellets diameter was 10-12mm. The experimental results are shown in **Figure 7**. For reducing at the condition of $H_2/(H_2+CO)$=0 for 150 min, the reduction degree of VTM pellets is only 72.6%. As the ratio of $H_2/(H_2+CO)$ increased to 1, the reduction degree of VTM pellets increased to 92.1%. It reveals that the reduction degree of VTM pellets increases with the increase of $H_2/(H_2+CO)$ ratio. Previous researches have confirmed that H_2 has higher reduction capacity and utilization than CO at high temperature (T>1084 K) [21,22].

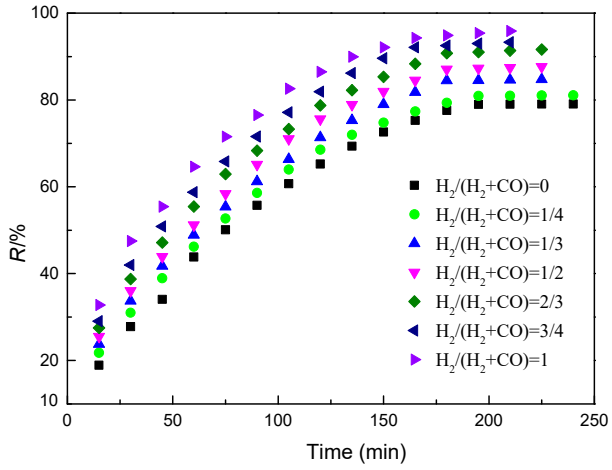

Figure 7. The reduction degree curves of oxidized VTM pellets at 1273K with $H_2/(H_2+CO)$ ratios.

Figure 8 presents the XDR patterns of the reduction VTM pellets products, which were obtained after reduced by the reduction gas with different $H_2/(H_2+CO)$ ratios at 1273K for 240min. It indicates that when the proportion of $H_2/(H_2+CO)$ is small, the phase of Fe_2TiO_5 disappeared and the main phase of the reduction product was $FeTiO_3$. The most probable reaction mechanism are Eq. (11), Eq. (12), Eq. (13), and Eq. (14). As the ratio of $H_2/(H_2+CO)$ increases to 2, $FeTiO_3$ is reduced to $FeTi_2O_5$. The most probable reactions are Eq. (15), and Eq. (16).

Preprints (www.preprints.org) | NOT PEER-REVIEWED | Posted: 30 October 2018 doi:10.20944/preprints201810.0723.v1

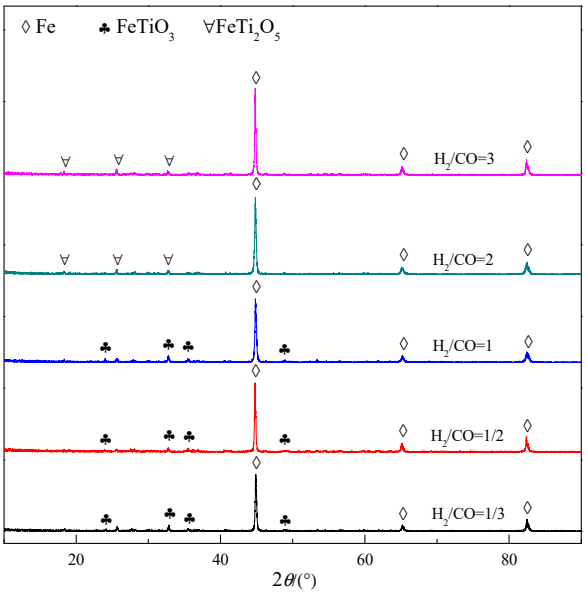

Figure 8. XRD patterns of reduction products at 1273K with $H_2/(H_2+CO)$ ratios.

Figure 9(a) and **(b)** show the Plot of $1-(1-R)^{\frac{1}{3}}$ vs. time and plot of $1-\frac{2}{3}R-(1-R)^{\frac{2}{3}}$ vs. time at 1273K in different $H_2/(H_2+CO)$ ratios atmosphere, respectively. There are also both the early stage and the latter stage, which are controlled by interface chemical reaction and diffusion, respectively. It reveals that the diffusion-control step was significantly shortened as the ratio of $H_2/(CO+H_2)$ increases. Therefore, the kinetic condition of reduction can be improved at 1273K with $H_2/(H_2+CO)$ ratios increasing. The hydrogen-rich reduction gas is definitely beneficial to the reduction of oxidized VTM pellets in the actual industrial production.

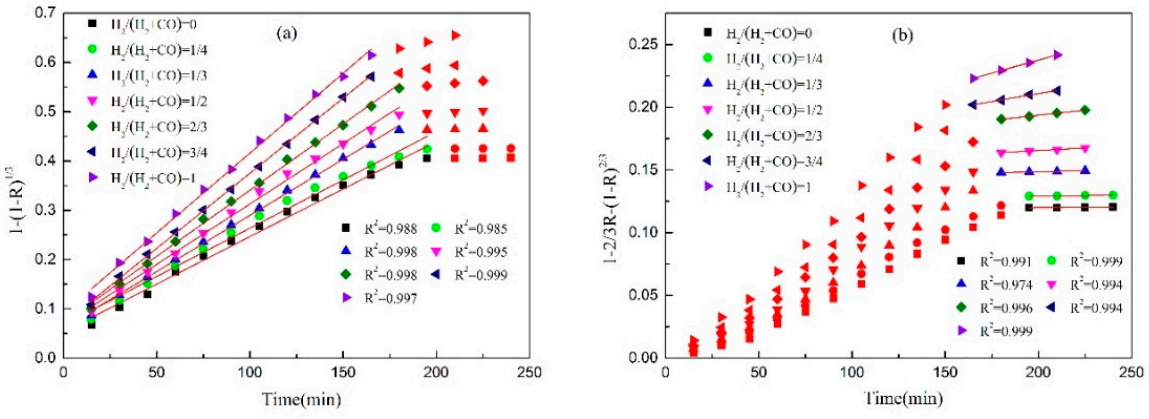

Figure 9. The reduction degree curves of oxidized VTM pellets at 1273K with $H_2/(H_2+CO)$ ratios.

3.3. Pellet size

To investigate the effect of pellet size on the reduction of oxidized VTM pellets, the reduction experiments were carried out under the condition with the oxidized VTM pellets diameter of 6-8mm, 8-10mm, 10-12mm, 12-14mm, and 14-16mm. Other specific experimental conditions were controlled: the reduction temperature was 1273K, the total gas flow was 5L·min^{-1}, the proportion of N_2 was 25%, the proportion of H_2 and CO was 75% (the $H_2/(H_2+CO)$=1/2).

Preprints (www.preprints.org) | NOT PEER-REVIEWED | Posted: 30 October 2018 doi:10.20944/preprints201810.0723.v1

As the pellet size changed from 6-8mm to 14-16mm, the reduction degree of the oxidized VTM pellets is shown in **Figure 10**. It can be seen that the pellet size of oxidized VTM pellets has a great influence on the reduction degree. The reduction degree increases with the decrease of the pellet size.

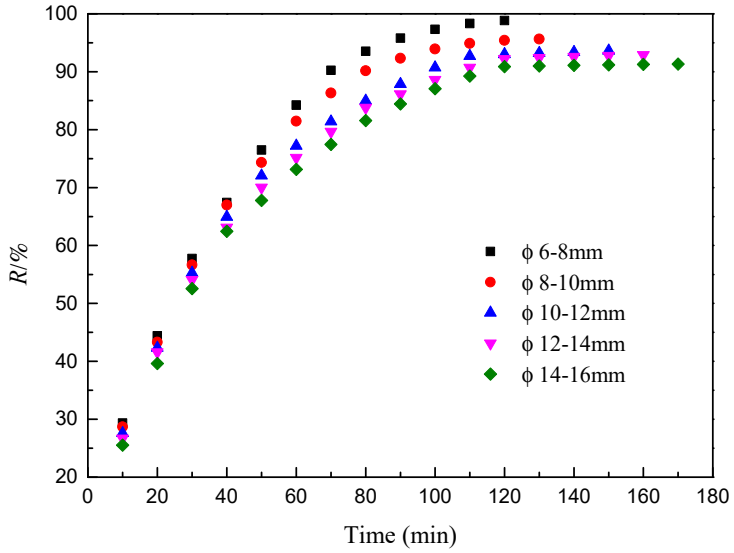

Figure 10. The reduction degree curves of oxidized VTM pellets at 1273K with different oxidized VTM pellets diameter in $H_2/(H_2+CO)$=1/2 atmosphere.

Figure 11 shows the XRD patterns of the reduction VTM pellets products, which were obtained at 1273K for 240min in $H_2/(H_2+CO)$=1/2 atmosphere. It can be seen that the phase of $FeTiO_3$ can be transferred into that of Fe_2TiO_5 with the decrease of pellets diameter. The most probable reaction mechanism can be described in Eq. (11), Eq. (12), Eq. (13), and Eq. (14). Until the pellet size decreases to Φ10-12mm, $FeTiO_3$ is reduced to $FeTi_2O_5$. The most probable reactions are Eq. (15), and Eq. (16). With the continuous decrease of pellet size, the diffractive peaks of $FeTi_2O_5$ are getting weaker and the peak metallic iron getting stronger, resulting in the enhancement of reduction degree.

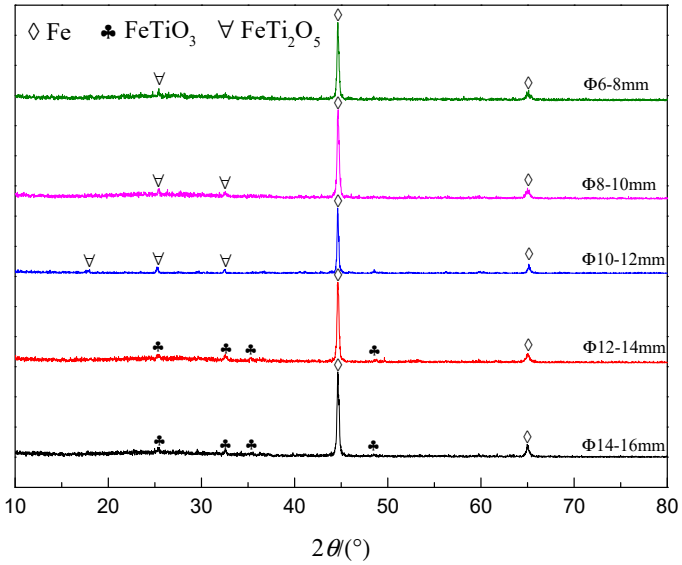

Figure 11. The reduction degree curves of oxidized VTM pellets at 1273K with different oxidized VTM pellets diameter in $H_2/(H_2+CO)$=1/2 atmosphere.

Preprints (www.preprints.org) | NOT PEER-REVIEWED | Posted: 30 October 2018 doi:10.20944/preprints201810.0723.v1

Figure 12 (a) and **(b)** show the Plots of $1-(1-R)^{\frac{1}{3}}$ and $1-\frac{2}{3}R-(1-R)^{\frac{2}{3}}$ vs. time with different oxidized VTM pellets diameter. It is obvious that early stage and the latter stage also exists during the reduction process, which are controlled by interface chemical reaction and diffusion, respectively. It is can be seen that the pellet size has great influence on the latter stage. The thickness of the product can be decreased with the decrease of pellet size during the reduction process. And diffusion degree of gas decreased quickly with the thickness of product layer increasing. This result presents that the diffusion-control step can be shortened with the decrease of the pellet size. Therefore, it is of great significance for optimizing the reduction process to select the appropriate pellet size. According to **Figure 12**, the values of reaction rate constant can be obtained and showed in **Table 3**. It indicates that the kinetic condition of reduction can be improved at 1273K in H_2 /(H_2+CO)=1/2 atmosphere with the decrease of the pellet size.

Table 3. The values of the reduction rate constant at 1273 K with different oxidized VTM pellets diameter.

pellets diameter	6-8mm	8-10mm	10-12mm	12-14mm	14-16mm
intrinsic chemical reaction control	0.00694	0.0057	0.00469	0.00423	0.00405
diffusion control	1.66E-03	6.35E-04	2.12E-04	1.58E-04	7.64E-05

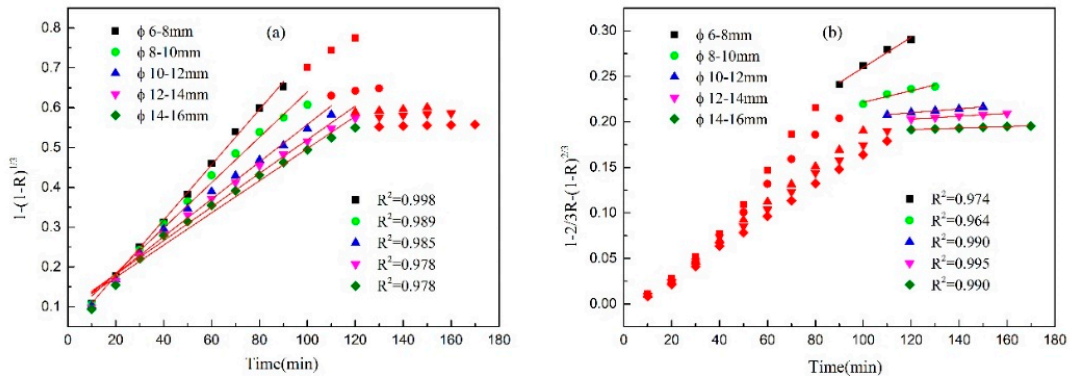

Figure 12. Plot of $1-(1-R)^{\frac{1}{3}}$ vs. time (a) and plot of $1-\frac{2}{3}R-(1-R)^{\frac{2}{3}}$ vs. time (b) at 1273K with different oxidized VTM pellets diameter in H_2/(H_2+CO)=1/2 atmosphere.

4. Conclusions

Gas-based reduction of oxidized VTM pellets in the mixture of H_2, CO, and N_2 was investigated at 973-1373K systematically. The reduction degree increases with the increase of reduction time, reduction temperature, H_2/(H_2+CO) ratios, but the decrease of pellet size. The Ti-bearing main mineral phase transformation of oxidized VTM pellets in H_2/(H_2+CO)=1/2 atmosphere is described as Fe_2TiO_5 → Fe_2TiO_4 → $FeTiO_3$ → $FeTi_2O_5$ with the reduction temperature increasing. And the Ti-bearing main mineral phase transformation of the reduction VTM pellets products at 1273K is described as Fe_2TiO_5 → $FeTiO_3$ → $FeTi_2O_5$ with the increase of H_2/(H_2+CO) ratios and the decrease of pellet size. The most probable reaction mechanism is provided based on the reduction process. The kinetics of oxidized VTM pellet in the reduction process is successfully modeled as a shrinking unreacted-core. In the whole reduction process, the kinetics study indicates that there are both the early stage and the latter stage, which are controlled by interface chemical reaction and diffusion, respectively. Besides, the diffusion-control step can be observably shortened with the decrease of pellet size because the thickness of the product layer becomes thinner in the reduction process.

Author Contributions: Conceptualization, Junwei Chen; Data curation, Junwei Chen; Formal analysis, Liang Mi; Funding acquisition, Xidong Wang; Investigation, Xidong Wang; Methodology, Junwei Chen; Project administration, Yang Jiao; Resources, Xidong Wang; Software, Yang Jiao; Supervision, Xidong Wang;

Validation, Xidong Wang; Visualization, Liang Mi; Writing – original draft, Junwei Chen; Writing – review & editing, Junwei Chen.

Funding: This work was supported by the ministry of land and resources public welfare industry research project (201511062-02).

Conflicts of Interest: The authors declare no conflict of interest.

References

1. Alfantazi A.M.; Moskalyk R.R. Processing of indium: a review. *Minerals Engineering*,**2003**,16,687-694. https://doi.org/10.1016/S0892-6875(03)00168-7
2. Zhou L.H.; Zeng F H. Reduction mechanisms of vanadium–titanomagnetite–non-coking coal mixed pellet. *Ironmaking and Steelmaking*,**2014**,38,59-64. https://doi.org/10.1179/030192310X12816231892549
3. Lv, X.; Lun, Z.; Yin, J.; Bai, C.; Carbothermic reduction of vanadium titanomagnetite by microwave irradiation and smelting behavior. *Isij International*,**2013**,*53*,1115-1119. https://doi.org/10.2355/isijinternational.53.1115
4. Zheng, F.; Chen, F.; Guo, Y.; Jiang, T.; Travyanov, A. Y.; Qiu, G. Kinetics of hydrochloric acid leaching of titanium from titanium-bearing electric furnace slag. *JOM*,**2016**,68,1-9. https://doi.org/10.1007/s11837-015-1808-7
5. Sui, Y. L., Guo, Y. F., Jiang, T., Qiu, G. Z. Sticking behaviour of vanadium titano-magnetite oxidised pellets during gas-based reduction and its prevention. *Ironmaking and Steelmaking*,**2016**,*44*,185-192. https://doi.org/10.1080/03019233.2016.1200284
6. Chen, D. S., Song, B., Wang, L. N., Qi, T., Wang, Y., Wang, W. J. Solid state reduction of panzhihua titanomagnetite concentrates with pulverized coal. *Minerals Engineering*,**2011**,*24*,864-869. https://doi.org/10.1016/j.mineng.2011.03.018
7. Guo, Y. F., Gao, Y., Tao, J., Qiu, G. Z. Solid-state reduction behavior of panzhihua ilmenite. *Journal of Central South University*,**2010**,*41*,1639-1644.
8. Cao, M. M., Zhang, J. L., Xing, X. D., Wang, C. L., Bai, Y. N., Wen, Y. C. Reduction mechanism of vanadium titano-magnetite carbon composite pellets. *Iron and Steel*,**2012**,*47*,5-12. https://doi.org/10.13228/j.boyuan.issn0449-749x.2012.08.010
9. Sui, Y. L., Guo, Y. F., Jiang, T., Qiu, G. Z. Reduction kinetics of oxidized vanadium titano-magnetite pellets using carbon monoxide and hydrogen. *Journal of Alloys and Compounds*,**2017**,*706*,546-553. https://doi.org/10.1016/j.jallcom.2017.02.264
10. Sui, Y. L., Guo, Y. F., Jiang, T., Xie, X. L., Wang, S., Zheng, F. Q. Gas-based reduction of vanadium titano-magnetite concentrate: behavior and mechanisms. *International Journal of Minerals Metallurgy and Materials*,**2017**,*24*,10-17. https://doi.org/10.1007/s12613-017-1373-x
11. Zhu, Z., Zhang, W., Cheng, C. Y. A synergistic solvent extraction system for separating copper from iron in high chloride concentration solutions.*Hydrometallurgy*,**2012**,*113-114*,155-159. https://doi.org/10.1016/j.hydromet.2011.12.016
12. Liu, S. S., Guo, Y. F., Qiu, G. Z., Jiang, T., Chen, F. Preparation of ti-rich material from titanium slag by activation roasting followed by acid leaching.*Transactions of Nonferrous Metals Society of China*,**2013**,*23*,1174-1178. https://doi.org/10.1016/S1003-6326(13)62580-7
13. Tang, J., Chu M.S., Feng C., Tang, Y.T., Liu Z.G. Melting Separation Behavior and Mechanism of High-chromium Vanadium–bearing Titanomagnetite Metallized Pellet Got from Gas-based Direct Reduction. *ISIJ Int*.**2016**,56,210-219. https://doi.org/10.2355/isijinternational.ISIJINT-2015-448
14. Mehdizadeh, A. M., Klausner, J. F., Barde, A., Mei, R. Enhancement of thermochemical hydrogen production using an iron–silica magnetically stabilized porous structure.*International Journal of Hydrogen Energy*,**2012**,*37*,8954-8963. https://doi.org/10.1016/j.ijhydene.2012.02.189
15. Piotrowski, K., Mondal, K., Lorethova, H., Stonawski, L., Szymański, T., Wiltowski, T. Effect of gas composition on the kinetics of iron oxide reduction in a hydrogen production process. *International Journal of Hydrogen Energy*,**2005**,*30*,1543-1554. https://doi.org/10.1016/j.ijhydene.2004.10.013
16. Zhao, W., Chu, M., Wang, H., Liu, Z., Tang, J., Ying, Z. Volumetric shrinkage characteristics and kinetics analysis of vanadium titanomagnetite carbon composite hot briquette during isothermal reduction. *Isij International*,**2018**,*58*,823-832. https://doi.org/10.2355/isijinternational.ISIJINT-2017-650

17. Guo, D., Hu, M., Pu, C., Xiao, B., Hu, Z., Liu, S. Kinetics and mechanisms of direct reduction of iron ore-biomass composite pellets with hydrogen gas. *International Journal of Hydrogen Energy*,**2015**,*40*,4733-4740. https://doi.org/10.1016/j.ijhydene.2015.02.065
18. Huitu, K., Helle, M., Helle, H., Kekkonen, M., Saxén, H. Optimization of midrex direct reduced iron use in ore-based steelmaking. *Steel Research International*,2015,*86*,456-465. https://doi.org/10.1002/srin.201400091
19. Kromhout, J. A., Ludlow, V., Mckay, S., Normanton, A. S., Thalhammer, M., & Ors, F., et al. (2002). Physical properties of mould powders for slab casting. *Ironmaking & Steelmaking*, *29*(3), 191-193. https://doi.org/10.1179/030192302225004133
20. Li, W., Fu, G. Q., Chu, M. S., Zhu, M. Y. Oxidation induration process and kinetics of hongge vanadium titanium-bearing magnetite pellets. *Ironmaking and Steelmaking*,**2016**,*44*,294-303. https://doi.org/10.1080/03019233.2016.1210751
21. Sun, H. Y., Dong, X. J., She, X. F., Xue, Q. G., Wang, J. S. Reduction mechanism of titanomagnetite concentrate by carbon monoxide. *Journal of Mining and Metallurgy*,*2013*,*49*,263-270. https://doi.org/10.2298/JMMB121001020S
22. Huang, Z. C., Ling-Yun, Y. I., Hu, P., Jiang, T. Effects of roast temperature on properties of oxide pellets and its gas-based direct reduction. *Journal of Central South University*,2012,*43*,2889-2895.